

# On the accumulation of solid bodies in global turbulent protoplanetary disc models

Sébastien Fromang<sup>1\*</sup> & Richard P. Nelson

<sup>1</sup> *Astronomy Unit, Queen Mary, University of London, Mile End Road, London E1 4NS*

Accepted; Received; in original form;

## ABSTRACT

We study the migration of solid bodies in turbulent protoplanetary accretion discs by means of global MHD simulations. The bodies range in size from 5 centimetres up to 1 metre, and so include objects whose migration is expected to be the most rapid due to gas drag interaction with the disc. As they drift inward through the disc, some of them are trapped in regions where gas pressure maxima are created by long lived anticyclonic vortices. This accumulation is very efficient, locally increasing the dust-to-gas ratio by a factor  $> 100$  in some cases. We discuss the possible implications of this result for theories of planet formation.

**Key words:** Accretion, accretion discs - MHD - Methods: numerical - Planets and satellites: formation

## 1 INTRODUCTION

A crucial element of any planet formation theory is understanding how the dust component of protoplanetary discs builds up to form larger objects that eventually become planetesimals and planets. This has obvious relevance to the formation of rocky terrestrial planets and asteroids, and according to the core-accretion model of gas giant formation (e.g. Pollack et al. 1996), is a key stage in the formation of giant planets.

The growth and evolution of solid bodies of all sizes is therefore an important topic to study. A key issue relates to the growth and survivability of metre-sized objects, which are expected to undergo rapid inward migration due to gas drag (Weidenschilling 1977). Such bodies are predicted to migrate into the central star within  $\sim 100$  years of formation, raising questions about how planetary systems form at all. Models of planet formation in smooth, laminar protoplanetary discs, beginning with small dust grains that must grow through this size range, require a radially extended reservoir of solid matter to overcome this problem (e.g. Weidenschilling & Cuzzi 1993).

In this letter, we investigate the effect MHD turbulence resulting from the magneto-rotational instability (MRI) in the disc might have on the dynamics of such objects. It seems likely that the MRI is the source of turbulence which transports angular momentum in protoplanetary discs. The velocity and density fluctuations that result will modify the drag force exerted on solid bodies and will affect their dynamics. These fluctuations can range from being relatively

small variations, up to being substantial modifications of the disc radial profile caused by radial variations in the turbulent stresses (e.g. Hawley 2001; Steinacker & Papaloizou 2002).

Because of the global nature of this problem, in which solid bodies will drift through a substantial fraction of the disc radius, we set up global protoplanetary disc simulations. As in Papaloizou & Nelson (2003), we have developed cylindrical discs models to limit the large computational cost of these calculations. We note that there has been a recent study of this problem by Johansen, Klahr & Henning (2005), who find transient trapping of solid bodies in density maxima generated by MHD turbulence. The approach used in their study, however, was local rather than the global approach we have taken.

The plan of the paper is as follows. In section 2, we describe our numerical schemes, and in section 3 we describe our results. We discuss their consequences and limitations in section 4.

## 2 SIMULATIONS

### 2.1 Algorithms

Two similar MHD Eulerian codes were used to compute the simulations presented in this paper: GLOBAL (Hawley & Stone 1995) and NIRVANA (Ziegler & Yorke 1997). Both use finite difference techniques combined with the Constrained Transport algorithm to evolve the MHD equations. They differ, however, in their treatment of the solid phase: GLOBAL treats the solid bodies as a second fluid; NIRVANA treats the solid bodies as particles. This

\* E-mail:s.fromang@qmul.ac.uk

reflects the sizes of the objects considered in each of our simulations.

### 2.1.1 The two fluid approach

GLOBAL was extended to describe the dust particle evolution as a second, pressureless fluid. This second fluid interacts with the gas via the drag force exerted by the latter. The drag force  $\mathbf{F}_{drag}$  takes the form

$$\mathbf{F}_{drag} = \frac{m_p}{\tau_s}(\mathbf{v}_g - \mathbf{v}_d). \quad (1)$$

Here  $m_p$  is the mass of the particle,  $(\mathbf{v}_g - \mathbf{v}_d)$  is the gas velocity relative to the solid component, and  $\tau_s$  is the dust stopping time. The small dust particles examined using GLOBAL are in the Epstein regime, so  $\tau_s$  is defined by

$$\tau_s = \frac{\rho_s a}{\rho c_s}, \quad (2)$$

where  $\rho$  is the gas density,  $c_s$  the speed of sound,  $\rho_s$  the density of the dust particles and  $a$  their size. Because of the short stopping time of the small particles studied in this work, the effect of the drag force is computed implicitly.

### 2.1.2 The N-body approach

The two fluid approximation breaks down for large solid bodies, so we adapted NIRVANA to include coupling between the fluid and individual solid objects represented by particles. We consider metre-sized bodies, whose drag force interaction is given by Stokes Law for the disc parameters we have adopted. The stopping time,  $\tau_s$ , then becomes (e.g. Weidenschilling 1977)

$$\tau_s = \frac{2\rho_s a^2}{9\eta} \quad (3)$$

where  $\eta$  is the gas viscosity defined by

$$\eta \simeq \frac{\lambda c_s}{3} \rho \quad (4)$$

and the mean free path of molecules  $\lambda = (n_{\text{H}_2} \sigma_{\text{H}_2})^{-1}$ . We adopt a value of  $\sigma_{\text{H}_2} = 10^{-15} \text{ cm}^2$  for the collision cross section of molecular hydrogen, and assume that  $n_{\text{H}_2} = \rho/m_{\text{H}_2}$ , where  $m_{\text{H}_2}$  is the mass of a hydrogen molecule (e.g. Rafikov 2004). We employ linear interpolation, using information from the surrounding eight cells, to obtain relevant physical quantities at the location of the particles.

In one simulation performed (model N1), the particles interacted with the disc through the drag force only. A second simulation (model N2) was performed in which the particles also experienced gravitational interaction with the disc. In this case the axisymmetric component of disc self-gravity was included to ensure that the velocity difference between solid particles and the gas was computed correctly (see Fromang, Terquem & Nelson 2005 for a description of the implementation). Simulations of low mass planets in turbulent discs indicate that the gravitational interaction between embedded objects and the turbulent fluctuations can have important consequences for the orbital evolution (Nelson & Papaloizou 2004; Nelson 2005a). It is for this reason we computed run N2 to examine the effect this may have on the evolution of smaller bodies that also interact with the disc gas through the drag force.

Model	dust description	Number of dust particles	Resolution	Particle size (in cm)
G1	fluid	No particle	(260, 152, 44)	5
G2	fluid	No particle	(260, 152, 44)	25
N1	N-body	3000	(260, 604, 44)	100
N2	N-body	500	(260, 604, 44)	100

**Table 1.** Model parameters of the runs presented here: Column 1 gives the name of the model. The first two (G1 and G2) are performed with GLOBAL and the last two (N1 and N2) with NIRVANA. The algorithm used to evolve the dust component (fluid vs N-body) is described in column 2. For the particle approach, column 3 gives the number of dust particles used. Finally, column 4 gives the resolution of the run and column 5 the size of the solid bodies, in centimetres.

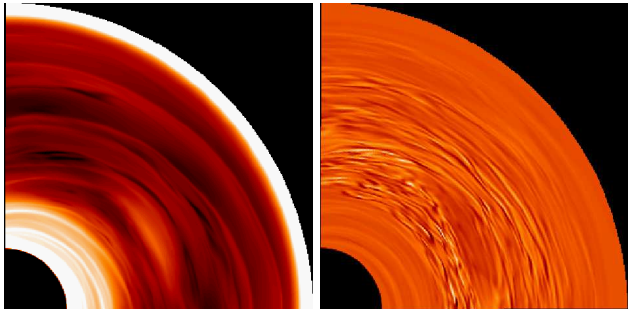


**Figure 1.** Logarithm of the density in the disc (*left panel*) and vorticity in the local rotating frame (*right panel*). Both quantities are calculated at the end of model G1. A region of negative vorticity is seen in the middle of the disc (at a location  $r \sim 2.5$  and  $\phi \sim \pi/6$ ), well correlated with a density increase on the left panel.

## 2.2 Model parameters

The parameters of the models that we computed here are described in table 1. We performed four models, labelled G1, G2, N1 and N2. They correspond to increasing particle sizes: 5 cm, 25 cm, and 1 m. The first two, for which there is good coupling between the gas and the dust, were computed with GLOBAL using the two fluid approach. In models N1 and N2 the large particles start to decouple from the gas, so the N-body approach implemented in NIRVANA was used. In the following, we describe the disc model parameters and the properties of the MHD turbulence that develops as a consequence of the MRI. We then describe the simulation results.

## 3 RESULTS

### 3.1 Disc model

The turbulent disc structure is computed following the procedure described in Nelson (2005a):  $\rho$  varies like  $r^{-1}$  and the equation of state is locally isothermal, with  $c_s \propto r^{-0.5}$ . The computational domain ranges in radius from  $R_{min} = 1$  to  $R_{max} = 5$  and its vertical extent is  $\Delta H = 0.28$ . In order to reduce the computational cost of models G1 and G2, the

azimuthal domain only covers the interval  $[0, \pi/2]$ . In that case, the resolution is  $(N_r, N_\phi, N_z) = (260, 152, 44)$ . In models N1 and N2, which cover the full azimuthal domain, the number of grid cells in  $\phi$  is four times larger.

When converting from computational to physical units, we assume that  $r = 2.3$  corresponds to 5 AU. The disc mass and density are scaled such that the total disc mass would be  $0.06 M_\odot$  within 40 AU (i.e. approximately three times the minimum mass nebula). The orbital period at the disc inner edge thus corresponds to  $\simeq 6$  years. We assume that the internal density of solid bodies  $\rho_s = 3 \text{ g cm}^{-3}$ .

In all of our models, turbulence is initiated in the disc with a non-zero net flux toroidal magnetic field. When the MRI starts to saturate, the field is scaled down by a factor of two, while the density profile is reset to its initial value (Nelson 2005a). The simulation is then restarted. This procedure gives a typical volume-averaged  $\alpha$  value computed from the Maxwell and Reynolds stress of  $\sim 10^{-2}$ . In both GLOBAL and NIRVANA, a quasi-steady state is obtained at  $t \simeq 300$  (measured throughout this paper in orbits at the inner edge of the disc), when the solid component is introduced. The turbulent state of the disc maintains a rough statistical steady state during the run time ( $\sim 180$ – $200$  orbits). The disc structure is illustrated by figure 1, where the left panel shows the density in the midplane of the disc at the end of model G1. A local increase in the density is visible in the middle of the disc. To better understand its nature, we plot in the right panel of figure 1 the vorticity  $\omega$  which is calculated at each radius in the local rotating frame according to:

$$\omega = \nabla \times \bar{\mathbf{v}}_g. \quad (5)$$

Here  $\bar{\mathbf{v}}_g$  is the difference between the local gas velocity and the azimuthally averaged velocity. White areas correspond to large positive values of  $\omega$  and dark zones to large negative values. A region with a lower value of  $\omega$  than the background of the disc is seen, which is well correlated with the density increase shown on the left panel. This is the signature of an anticyclonic vortex (Johansen & Klahr 2005). Note that the decrease in  $\omega$  that is created is of smaller amplitude than the vorticity fluctuations that result from the MHD turbulence. Similar vortices are observed in runs N1 and N2, and we observe these structures to survive for the duration of the simulations. Their nature and formation mechanism are discussed further and compared with previous work in section 4.

### 3.2 Models G1 and G2

At time  $t = 300$ , the dust is introduced such that  $\rho/\rho_d = 100$  everywhere in the disc and the evolution is followed until  $t = 477$ . The parameter  $\Omega\tau_s$  (where  $\Omega$  is the Keplerian angular velocity) is independent of radius in these models. Two cases are investigated. Model G1 corresponds to  $\Omega\tau_s = 0.1$ , and model G2 has  $\Omega\tau_s = 0.5$ . Given the model normalization described above, these parameters respectively correspond to solid bodies whose diameter is equal to 5 and 25 centimetres.

During the simulations, the dust drifts radially toward the central object and the spatial distribution evolves. The logarithm of the gas-to-dust ratio in the  $(r - \phi)$  plane is shown in figure 2 for model G1 (*left panel*) and G2 (*right*

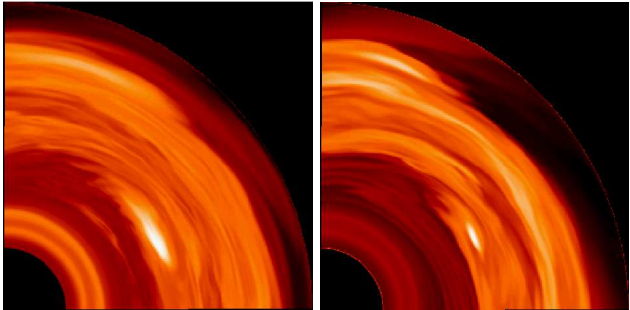


**Figure 2.** Logarithm of the dust-to-gas ratio at the end of model G1 (*left panel*) and G2 (*right panel*). Its maximum value respectively reaches 0.34 and 1.41.

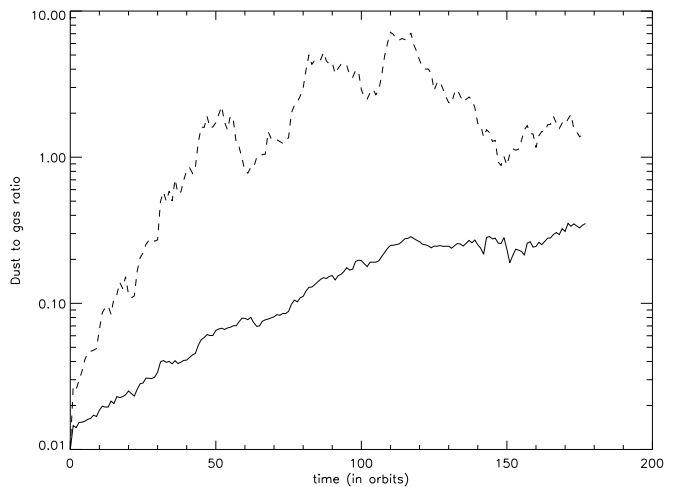


**Figure 3.** Time history of the maximum value reached by the gas to dust ratio for model G1 (*solid line*) and G2 (*dashed line*).

*panel*) at time  $t = 176$ . The striking feature of both of the snapshots is the accumulation of dust in a region of the disc close to  $r = 2.7$ . The peak value of the dust to gas ratio at that time is 0.34 and 1.41 for model G1 and G2, which indicates an increase of respectively 34 and 141 during the course of the simulation. A comparison between figures 1 and 2 shows that this accumulation occurs at a location corresponding to a local increase of the gas density (or, equivalently, of the gas pressure). We have shown in section 3.1 that this pressure extremum corresponds to an anticyclonic vortex. The fact that solid bodies are efficiently trapped in such a vortex has been previously reported in the literature on several occasions (Barge & Sommeria 1995; Godon & Livio 2000; Johansen et al. 2004). The novel result of our work is that this long-lived vortex is self-consistently generated by the MHD turbulence itself.

Finally, figure 3 plots the time history of the maximum value reached on the grid by the gas-to-dust ratio for models G1 and G2. Both curves show an increase with time. However, there is a clear tendency for larger particles to accumulate more quickly in gas pressure maxima, as they undergo faster radial migration, and the maximum value for the dust-to-gas ratio reached in model G2 is greater than

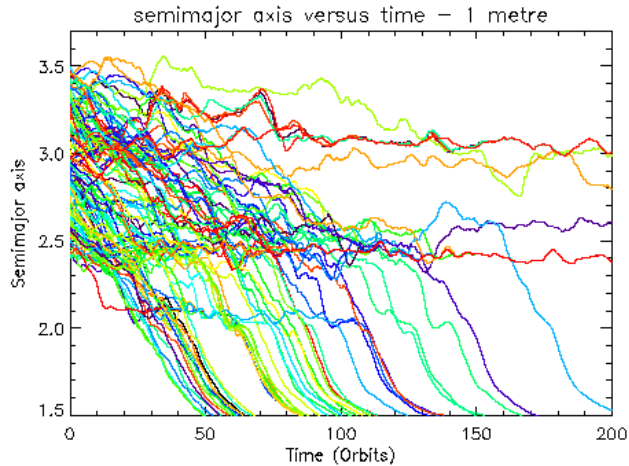


**Figure 4.** This figure shows the radial trajectories of 120 representative solid bodies from simulation N1. Note that there are two regions in the disc where particles are trapped, corresponding to local pressure maxima in the disc. Very similar results were obtained in simulation N2.

unity. In both models, the value of the dust-to-gas ratio saturates after about 120 orbits in model G1 and after 50 orbits in model G2. This is because the outer regions of the disc are depleted at that time and there is no more solid material to supply the region where dust accumulates.

### 3.3 Models N1 and N2

Simulations N1 and N2 employed 3000 and 500 particles, respectively, to trace the trajectories of 1 metre sized solid bodies. Their initial radial and azimuthal locations were distributed randomly in a narrow annulus between  $2.4 \leq r_p \leq 3.2$ , and they were initiated with Keplerian circular velocities. For the disc model we adopt, the stopping time for simulations N1 and N2 are given by  $\Omega\tau_s = 1.15 \left(\frac{r_p}{2.5}\right)^{-1}$ . Between radii 1.5 – 3.2,  $\Omega\tau_s$  thus ranges between  $\sim 1.92$  and 0.85. The radial trajectories of 120 particles from simulation N1 are shown in figure 4. The simulation ran for 200 orbits at the disc inner edge. The inward drift of particles due to gas drag is apparent. For those particles that undergo global migration through the disc, we find reasonable overall agreement in the migration time compared with that obtained in an equivalent laminar disc simulation. It is clear, however, that there are particles that do not undergo substantial inward drift over the simulation run time, but instead become trapped at specific radii. Figure 4 shows that there are four separate radii around which particles become concentrated. Most of these particles become trapped because they become concentrated in anticyclonic vortices that form in the turbulent flow, and maintain their identity for the duration of the simulation. For a given vortex, the trapped particles eventually find themselves being concentrated into a single grid cell, such that they then maintain very similar trajectories for the duration of the simulation.

Out of 3000 particles considered, 1356 migrate interior to  $r = 1.5$  after 200 orbits, without becoming trapped at intermediate radii. There are three distinct vortices that form in simulation N1 that lead to particles being concentrated.

One is located at radius  $r \simeq 2.4$ , and traps 1276 particles. Another vortex forms at radius  $r \simeq 2.6$ , and contains 24 particles. This vortex is observed to be weaker than the former one, explaining the reduced particle concentration. At the end of the simulation there are 3 particles orbiting at radii  $r \simeq 2.8$ , but these are not contained within an obvious vortex, but appear to be tail-enders whose inward drift has been disrupted through turbulence-induced perturbations. A third vortex orbits at  $r \simeq 3.0$ , and contains 341 particles at the end of the simulation. Statistically, we find that just under 50 percent of the particles migrate substantially through the disc, and just over 50 percent become concentrated within the vortices that form.

A similar picture emerges from run N2, which included the gravitational interaction between solid bodies and the disc. This simulation resulted in particles becoming concentrated in vortices at radii  $r \simeq 2.5$  and  $r \simeq 2.9$ . The degree of concentration was similar to that in run N1, with 40 percent of particles migrating interior to  $r = 1.5$  and 60 percent being concentrated further out in the disc. It is clear that gas drag dominates the evolution for 1 metre-sized bodies, with perturbations to their motion induced by disc gravity having little effect. Simulations that include larger bodies ( $a \geq 10$  metres) indicate that the concentration of solid bodies observed here does not hold for that size range, and that the disc gravity rapidly becomes the dominating influence on the orbital evolution of larger planetary building blocks (Nelson 2005b).

## 4 DISCUSSION

We have presented the results of MHD simulations of cylindrical accretion disc models that include the orbital evolution of solid bodies ranging in size from 5 centimetres to 1 metre. A two fluid approach was used for the 5 and 25 cm sized particles, and an N-body approach used for the 1 metre sized objects. Both methods were able to follow the radial drift of the solid bodies relative to the gas.

Two results emerge from these simulations: vortices were found to develop in the disc and to survive for the duration of the simulations, and dust was observed to accumulate very efficiently in these long-lived structures.

The first of these findings is significant as previous studies of MHD turbulence in cylindrical discs (Armitage 1998; Hawley 2001; Steinacker & Papaloizou 2002) have not reported long-lived vortices. The reason for this may be that these structures are difficult to identify in turbulent discs, because they tend to be weak in comparison with the transient background features. By-eye inspection of density plots often does not reveal vortices, and we found it necessary to inspect the vorticity before being convinced that vortices were indeed present in our models.

The issue of the formation and survival of vortices in discs is long-standing. Although it has been shown that anticyclonic vortices can survive for hundreds of orbits (Barge & Sommeria 1995; Godon & Livio 1999), few mechanisms have been put forward to explain their formation in a barotropic fluid. Godon & Livio (2000) suggested that small vortices resulting from underlying turbulence could merge to form larger, stable anticyclonic vortices. We find that turbulence generates small scale variations in vorticity,

and it is possible that some of the small scale regions of anticyclonic vorticity may merge to form longer lived structures. We find that early on in the simulations, when the disc is being relaxed prior to the dust component being added, larger patches of underlying vorticity also exist. These are not apparent against the higher amplitude background fluctuations, but become so if the magnetic field is switched off and the turbulence is allowed to decay. The disc returns to a laminar state, but with continued existence of the underlying vortices that are apparently responsible for trapping dust when it is added later to the simulations.

Another possible route to their formation is the Papaloizou–Pringle instability (Papaloizou & Pringle 1984). Hawley (1987) showed that radially–slender tori will break-up into gaseous blobs or “planets”. There is some evidence that the vortices formed in our discs occur near pressure and density maxima caused by radial variations in the viscous stress. It remains an open question whether these radial density variations are susceptible to this instability, causing the vortices we observe to form. A detailed analysis of the origin of the vortices goes beyond the scope of this *letter*, and we note that Barranco & Marcus (2005) have suggested that vortices are unstable when vertical stratification is included. The equation of state may also be of some importance (see, for example, Klahr & Bodenheimer 2003). We will examine these issues in a future paper.

The second result presented in this letter is that solid bodies in the size range considered concentrate efficiently in regions of the disc where pressure maxima form due to the anticyclonic vortices described above. This accumulation is a well know process that has been studied before (Barge & Sommeria 1995; Godon & Livio 2000; Johansen et al. 2004). The two fluid calculations demonstrated that the effect of trapping was more pronounced for the 30 centimetre sized objects than for the 5 centimetre ones because of their more rapid inward drift. A simulation performed for 1 metre sized bodies including the effects of the disc gravity demonstrated that gas drag forces are very dominant in determining the evolution for these size ranges. All simulations indicated that the trapping was very efficient, with between 50 – 75 percent of the solids surviving inward migration through the full extent of the disc over runs times of  $\sim 200$  orbits. Test calculations using laminar disc models showed complete loss of solid bodies with sizes in the range considered here.

Note that we did not include the back reaction of the solids on the gas in this work, which is valid only in regions where the gas density is much larger than the solid density. Large enhancements in the density of solids mean that the local dynamics may become dominated by the solid bodies rather than gas. It will be necessary to include the back reaction of the solids on the gas in future studies to investigate this effect.

In the N-body approach, finite resolution effects tend to cause particles to clump together on the grid-scale, and it is for this reason that we have not quoted density enhancement factors for these runs. This issue can be addressed by adopting a sub grid scale model for the turbulence.

The effect of trapping presented in this letter may help overcome the problem of very rapid migration of intermediate sized bodies during planet formation (e.g. Weidenschilling 1977). The enhanced concentration arising

from this trapping will very likely lead to an enhanced growth rate of the solid bodies involved *via* binary sticking, though the sticking presumably occurs between larger bodies and smaller grains that are trapped in the same region, given the difficulty of sticking macroscopic objects together. This will allow bodies to grow to sizes for which the inward migration is much less rapid. Indeed simulations of larger bodies in turbulent discs suggest that objects larger than 10 metres no longer have their evolution controlled by gas drag but rather through gravitational interaction with turbulent density fluctuations (Nelson 2005b).

## ACKNOWLEDGMENTS

The simulations presented in this paper were performed on the U.K. Astrophysical Fluid Facilities (UKAFF) and on the QMUL High Performance Computing Facility purchased under the SRIF initiative. The authors thank Laure Barrière-Fouchet for her help in setting up the two fluids description used in GLOBAL. We also acknowledge comments provided by the referee, Hubert Klahr, that have improved this paper.

## REFERENCES

- Armitage P. J., 1998, *ApJ*, 501, L189
- Barge P., Sommeria J., 1995, *A&A*, 295, L1
- Barranco J. A., Marcus P. S., 2005, *ApJ*, 623, 1157
- Fromang S., Terquem C., Nelson R., 2005, *MNRAS*
- Godon P., Livio M., 1999, *Apj*, 523, 350
- Godon P., Livio M., 2000, *Apj*, 537, 396
- Hawley J., Stone J., 1995, *Comput. Phys. Commun.*, 89, 127
- Hawley J. F., 1987, *MNRAS*, 225, 677
- Hawley J. F., 2001, *ApJ*, 554, 534
- Johansen A., Andersen A. C., Brandenburg A., 2004, *A&A*, 417, 361
- Johansen A., Klahr H., 2005, *ApJ*
- Johansen A., Klahr H., Henning T., 2005, *ApJ*
- Klahr H. H., Bodenheimer P., 2003, *ApJ*, 582, 869
- Nelson R., 2005a, *A&A*
- Nelson R., 2005b, *A&A*
- Nelson R., Papaloizou J., 2004, *MNRAS*, 350, 849
- Papaloizou J., Nelson R., 2003, *MNRAS*, 339, 983
- Papaloizou J. C. B., Pringle J. E., 1984, *MNRAS*, 208, 721
- Rafikov R. R., 2004, *AJ*, 128, 1348
- Steinacker A., Papaloizou J., 2002, *ApJ*, 571, 413
- Weidenschilling S. J., 1977, *MNRAS*, 180, 57
- Weidenschilling S. J., Cuzzi J. N., 1993, in *Protostars and Planets III Formation of lanetesimals in the solar nebula.* pp 1031–1060
- Ziegler U., Yorke H. W., 1997, *Computer Physics Communications*, 101, 54